Structural Engineering and Mechanics, *Vol. 68, No. 5 (2018) 603-619*
DOI: https://doi.org/10.12989/sem.2018.68.5.603

Domain decomposition technique to simulate crack in nonlinear analysis of initially imperfect laminates

S. Amir M. Ghannadpour* and Mona Karimi

Faculty of New Technologies and Engineering, Shahid Beheshti University, G.C, Tehran, Iran

(Received June 30, 2018, Revised August 9, 2018, Accepted October 23, 2018)

Abstract. In this research, an effective computational technique is carried out for nonlinear and post-buckling analyses of cracked imperfect composite plates. The laminated plates are assumed to be moderately thick so that the analysis can be carried out based on the first-order shear deformation theory. Geometric non-linearity is introduced in the way of von-Karman assumptions for the strain-displacement equations. The Ritz technique is applied using Legendre polynomials for the primary variable approximations. The crack is modeled by partitioning the entire domain of the plates into several sub-plates and therefore the plate decomposition technique is implemented in this research. The penalty technique is used for imposing the interface continuity between the sub-plates. Different out-of-plane essential boundary conditions such as clamp, simply support or free conditions will be assumed in this research by defining the relevant displacement functions. For in-plane boundary conditions, lateral expansions of the unloaded edges are completely free while the loaded edges are assumed to move straight but restricted to move laterally. With the formulation presented here, the plates can be subjected to biaxial compressive loads, therefore a sensitivity analysis is performed with respect to the applied load direction, along the parallel or perpendicular to the crack axis. The integrals of potential energy are numerically computed using Gauss-Lobatto quadrature formulas to get adequate accuracy. Then, the obtained non-linear system of equations is solved by the Newton-Raphson method. Finally, the results are presented to show the influence of crack length, various locations of crack, load direction, boundary conditions and different values of initial imperfection on nonlinear and post-buckling behavior of laminates.

Keywords: geometric nonlinearity; crack; plate decomposition technique; ritz; penalty technique; composite plates

1. Introduction

Thin-walled structures have widely used in various structural components such as aerospace structures. Plates which are made from the fiber reinforced composite materials have been preferred than other materials because they are lightweight and strong. These structures are mostly subjected to in-plane compressive loads. Composite plates can withstand under mechanical loads more than the buckling load and for this reason many researchers have investigated the behavior of these structures after the buckling which is called post-buckling regime. However, applying these loads may cause failures such as cracks, which will reduce the ultimate strength of the composite plates. Understanding the nonlinear and post-buckling behaviors of these structures that contain crack are very important in the design procedure.

In the field of plates without the cracks, extensive research has been done to study the post-buckling behavior of various kinds of plates that is rapidly developing. A comprehensive review in the field of buckling and post-buckling until 1988 can be found in Chia (1988) and Leissa (1987). Many researchers have recently analyzed the buckling, post-buckling and nonlinear behaviors of functionally graded and composite structures under different loading conditions using finite element method (FEM), finite strip method (FSM) and some semi-analytical methods. For example, one can refer to the works done by Panda and Singh (2013a), Cetkovic and Vuksanovic. (2011), Ghannadpour *et al.* (2018) and Ovesy and Ghannadpour (2009, 2011). Also, Panda and Singh (2009, 2010a, b, 2011, 2013b, c), Panda and Katariya (2015) and Katariya and Panda (2016) have investigated the buckling and post-buckling behavior of composite panels, spherical and cylindrical shells under thermo-mechanical loading using nonlinear finite element method. Katariya *et al.* (2017a, b, 2018) have studied on thermal buckling strength of laminated sandwich composite panels with or without shape memory alloy. Kar and Panda (2016, 2017) have analyzed the post-buckling behavior of FG curved shells under edge compression and non-uniform thermal loading. Also, Kar *et al.* (2016, 2017) and Panda *et al.* (2017) have studied on thermal buckling and post-buckling of FG doubly curved shells and FG panel structures using finite element method. Ghannadpour and his co-workers (2015, 2016) developed a new exact finite strip based on First-order Shear Deformation plate Theory (FSDT) to study the buckling and post-buckling behavior of shear-deformable composite plates. Kandasamy *et al.* (2016) analyzed the buckling and post-buckling behavior of moderately thick laminated rectangular plates by FSDT and Panda and Ramachanda (2011) has studied the buckling and post-

*Corresponding author, Ph.D.
E-mail: a_ghannadpour@sbu.ac.ir

http://www.techno-press.com/journals/sem&subpage=7 ISSN: 1225-4568 (Print), 1598-6217 (Online)

buckling of cross-ply composite plates subjected to non-uniform in-plane loads.

Composite plates are prone to suffer various types of defects such as delaminations and cracks (Liu *et al.* 2015). The cracks may affect the load carrying capacity of the laminated plates and plate structures. The presence of cracks in the structure may also cause stiffness reduction of the structure. This reduction in stiffness becomes more pronounced especially after buckling and in the post-buckling region. Therefore, it is necessary to investigate the buckling, post-buckling and geometrically nonlinear behaviors of cracked composite plates. A few studies have also been conducted in this regard, which can be summarized as follows. It should be emphasized that most analyses of composite plates are usually carried out using FEM in which the storage required is extremely large, and the computational time is too lengthy (Rangarajan and Gao 2015). Only a limited number of such analyses have been implemented by other numerical or semi-analytical methods (Kress and Lee 2003, Monfared 2017). Cao and Liu (2012) developed isoparametric element method to solve 3-D crack problem by constructing a new displacement modeling. In some research studies, the generalized differential quadrature finite element method is introduced and used to examine the static and dynamic behavior of cracked structures such as Viola *et al.* (2013a, b), Fantuzzi *et al.* (2016) and Shahverdi and Navardi (2017). Alinia *et al.* (2007) investigated the linear and non-linear buckling behavior of shear panels that have cracks edge; cracks are parallel or normal to the boundary. Nasirmanesh and Mohammadi (2015) have shown the effects of crack length and angle, fiber directions and boundary conditions on the buckling behavior of cracked composite plate with compressive, tensile and shear loadings. In some references such as Yuan and Dickinson (1992), cracks have been modeled as a series of line springs.

Experimental and numerical buckling analyses of cracked plates under various loadings conditions were performed by Seifi and Khodayari (2011) and Seifi and Kabiri (2013). More recently, Milazzo and Oliveri (2015) investigated the post-buckling behavior of cracked composite plates without initial imperfection effects by using plate assembly technique and also delaminated stiffened panel (Milazzo and Oliveri 2017). Dimitri *et al.* (2017) using numerical extended finite element method (XFEM) have predicted the fraction direction of propagation within a specimen, and calculated the stress intensity factor for cracked plate under different loading conditions. Some researchers used mesh less formulation to solve cracked problems. Batra and Ching (2002) have analyzed transient deformation near a crack by meshless local Petrov-Galarkin (MLPG) method. Peng *et al.* (2017) have simulated the stiffened plate with edge crack by FSDT and MLS[1] approximation based on mesh less formulation.

The aim of this paper is to study the effects of crack length and location, various boundary conditions, load direction and initial imperfection on the nonlinear and post-buckling behaviors of composite plates by a novel semi-analytical method. The laminated plates are decomposed into six sub-plates and therefore the plate decomposition technique is used in this research. The connection between the sub-plates is established by the penalty technique. The Ritz method is used to model the problem and the strain-displacement relationships are written based on the FSDT. In order to approximate the primary variables, Legendre basis functions are used here. Different out-of-plane essential boundary conditions such as clamp, simply support and free conditions will be assumed in this research by defining the relevant displacement fields. For in-plane boundary conditions, lateral expansion of the unloaded edges is free while the loaded edges are assumed to move straight but restricted to move laterally. The laminated plates are assumed to be subjected to biaxial compressive loads, therefore a sensitivity analysis is performed with respect to the applied load direction, along the parallel or perpendicular to the crack axis. By using the principle of minimum of total potential energy, the nonlinear equilibrium equations are obtained and solved by Newton-Raphson technique. It is noted that the integrals of potential energy are numerically computed by Gauss-Lobatto quadrature formulas to get adequate accuracy.

[1]Moving least-square

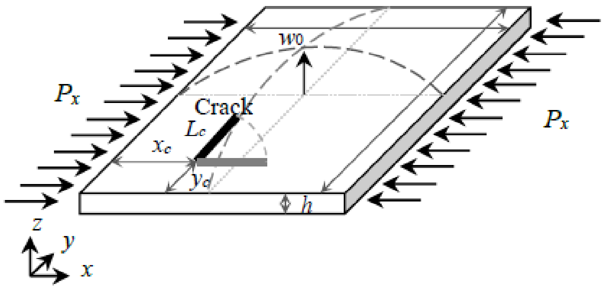

Fig. 1 Plate geometry model and loading

2. Model geometry and boundary conditions

Laminated plates with dimensions $A \times B$ and total thickness $h$are considered in this study as shown in Fig. 1. As it can be seen, an initial geometric imperfection w_0 at the center of the plate and in the z-direction is also assumed in the plate under consideration. In accordance with the aim of this study, a crack with length L_c has been located at (x_c, y_c) from the origin of the coordinates and in the domain Ω .The laminates are subjected to in-plane compressive load P_x along the x-direction (or P_y along the y-direction which is not shown in the figure due to simplicity). The laminates are assumed to be moderately thick, thus the formulations are based on the first order shear deformation theory (FSDT).

Different out-of-plane essential boundary conditions such as clamp, simply support and free conditions will be assumed in this research by defining the relevant displacement fields in the next section. However, for in-plane boundary conditions, lateral expansion of unloaded edges is free while the loaded edges are assumed to move straight (Fig. 2). It is also noted that the loaded edges of the

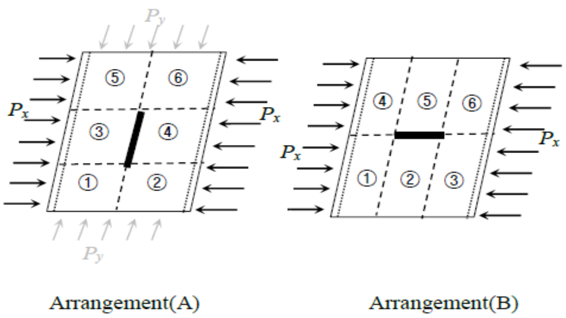

Fig. 2 Plate decomposition configurations

plates are restricted to move laterally.

To model the crack, the entire domain of the laminates is partitioned into several sub-plates and therefore, a plate decomposition technique is used. In this technique and in the present research, the laminated plates under considerations are decomposed into six sub-plates as shown in Fig. 2(a). As it can be seen, in this decomposition configuration where the six sub-plates are arranged laterally, the direction of the applied load P_x is orthogonal to the crack axis. To investigate the nonlinear behavior of cracked plates with cracks along the loading direction, one can change the direction of the applied load from longitudinal to lateral direction (P_y) with transferring the boundary conditions between two directions or model the plate as shown in Fig. 2(b). In this type of decomposition, it is observed that the six sub-plates have been arranged longitudinally. Both methods are used in this paper.

In the above figures, the sub-plates with domains $\Omega^{(i)}$ have dimensions $a^{(i)} \times b^{(i)}, i = 1,2,\ldots,6$ and thickness h. After decomposition, with regard to the specified boundary conditions of the plate, the displacement fields should be considered for each sub-plate. It is noted that for the edges shared between contiguous elements, since the displacements are unknown, therefore free boundary conditions should be assumed. After selecting appropriate displacement fields, the sub-plates should be assembled by using a relevant technique to model the crack in the laminated plates. In this study, penalty technique is used to enforce interface continuity between the sub-plates. As it is known, in arrangement A, sub-plates 3 and 4, and in arrangement B, sub-plates 2 and 5 have no connection to each other to accurately model the crack in the plate.

The development of the formulation of this study, including the approximation of displacement fields for each sub-plate, calculating the total potential energy of the sub-plates and using the penalty technique, are presented in the next section.

3. Formulations

As mentioned before, the imperfect laminated plates in this study are under compressive loads and therefore they undergo deformations. Each point in the domain of the plates with the position vector $\boldsymbol{x} = \langle x \quad y \quad z\rangle^T$ is transferred to a new coordinate value $\boldsymbol{x}^* = \langle x^* \quad y^* \quad z^*\rangle^T$ by

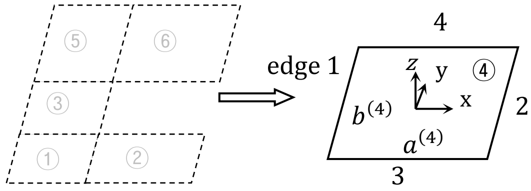

Fig. 3 Plate and sub-plates geometry models

$$\boldsymbol{x}^* = \boldsymbol{x} + \boldsymbol{u} \tag{1}$$

Where $\boldsymbol{u} = \langle \bar{u} \quad \bar{v} \quad \bar{w}\rangle^T$ is displacement vector and describes the deformation of a laminated plate whose components are given by

$$\begin{aligned} \bar{u}(x,y,z) &= u(x,y) + z\varphi_x(x,y) \\ \bar{v}(x,y,z) &= v(x,y) + z\varphi_y(x,y) \\ \bar{w}(x,y,z) &= w(x,y) + w_I(x,y) \end{aligned} \tag{2}$$

According to the FSDT, u, v and w are in-plane and out-of-plane displacements of mid-plane, and $\varphi_x$and φ_y denote the rotations of a transverse normal about axes parallel to the$x$ and y axes, respectively. As it is seen, since the plates have initial geometric imperfection w_I in the z-direction, therefore the effect of this imperfection is also included in the third equation of relations (2).

In order to investigate the behavior of laminated plates, all above displacement fieldsu, v, $w, \varphi_x$and $\varphi_y$should be approximated in the domain of the plates and since the entire domain is partitioned into several sub-plates, therefore the above displacement fields should be approximated separately for each sub-plate. According to the mentioned boundary conditions in section 2, displacement fields can be written as

$$\begin{aligned} &\tau^{(i)}(x,y) \\ &= \mathbb{B}_\tau^{(i)}(x,y) \sum_{m=1}^{N_t} \sum_{n=1}^{N_t} \delta_{mn}^{\tau^{(i)}} P_{m-1}\left(\frac{2x}{a^{(i)}}\right) P_{n-1}\left(\frac{2y}{b^{(i)}}\right) \\ &+ f_\tau^{(i)}(x,y)\delta_c^{\tau^{(i)}}, \quad i = 1,2,\ldots,6 \end{aligned} \tag{3}$$

Where $\tau \in \{u, v, w, \varphi_x, \varphi_y\}$ is a selected displacement field for $(i)^{th}$ sub-plate and$N_t$is the number of terms in series expansion which is taken same for all displacement fields and sub-plates in this paper and m and n are positive integers. The coefficients $\delta_{mn}^\tau$and δ_c^τ are the Ritz unknown coefficients of the problem for each sub-plate (i) and the latter is for satisfying the straight conditions. It is noted that the origin of the coordinates for each sub-plate is assumed to be at its center as in Fig. 3.

The so-called boundary function $\mathbb{B}_\tau(x,y)$ is chosen to ensure the fulfillment of the essential boundary conditions of each sub-plate (i). It can be defined as

$$\begin{aligned} \mathbb{B}_\tau^{(i)}(x,y) = \prod_{\beta=1,2} \left(1 + (-1)^{\beta-1}\left(\frac{2x}{a^{(i)}}\right)\right)^{\mu_\beta^{\tau^{(i)}}} \prod_{\beta=3,4} \Bigg(1 \\ + (-1)^{\beta-1}\left(\frac{2y}{b^{(i)}}\right)\Bigg)^{\mu_\beta^{\tau^{(i)}}}, i = 1,\ldots,6 \end{aligned} \tag{4}$$

Where β denotes the edge number and the exponents $\mu_{\beta}^{\tau(i)}$ can take the value 0 for free condition and the value 1 according to the conditions of held (or straight) for each displacement field $\tau \in \{u, v, w, \varphi_x, \varphi_y\}$ and for each sub-plate.

The boundary function $f_{\tau}^{(i)}(x, y)$ is also chosen to ensure the fulfillment of the straight boundary conditions of the plates as mentioned in previous section. Therefore, since this specified boundary condition is only related to the in-plane displacement fields $\tau \in \{u, v\}$ depending on the direction of applied load; the value of this function is zero for other displacement fields $\tau \in \{w, \varphi_x, \varphi_y\}$.

As it is seen in Eq. (3), the approximation of displacement fields is performed by Legendre basis functions P. Legendre polynomials are one of the most powerful mathematical series of numerical methods. Legendre basis functions or Legendre polynomials are solutions to the following Legendre differential equation

$$\frac{d}{dx}\left[(1-x^2)\frac{d}{dx}P_n(x)\right] + n(n+1)P_n(x) = 0 \tag{5}$$

Also, Legendre polynomials satisfy the three-term recursion as

$$P_{n+1}(x) = \frac{2n+1}{n+1}xP_n(x) - \frac{n}{n+1}P_{n-1}(x) \tag{6}$$

Where $P_0(x) = 1$and$P_1(x) = x$.

By approximating the displacement functions as described above, the in-plane strain vectors for each sub-plate can be represented by the following relationships.

$$\bar{\boldsymbol{\varepsilon}}^{(i)} = \begin{Bmatrix} \bar{\varepsilon}_{xx}^{(i)} \\ \bar{\varepsilon}_{yy}^{(i)} \\ \bar{\varepsilon}_{xy}^{(i)} \end{Bmatrix} = \boldsymbol{\varepsilon}^{(i)} + z\boldsymbol{\psi}^{(i)}, \quad \boldsymbol{\varepsilon}^{(i)} = \begin{Bmatrix} \varepsilon_{xx}^{(i)} \\ \varepsilon_{yy}^{(i)} \\ \varepsilon_{xy}^{(i)} \end{Bmatrix} = \boldsymbol{\varepsilon}_{\boldsymbol{l}}^{(i)} + \boldsymbol{\varepsilon}_{\boldsymbol{nl}}^{(i)} + \boldsymbol{\varepsilon}_{\boldsymbol{I}}^{(i)} \tag{7}$$

where $\boldsymbol{\varepsilon}_{\boldsymbol{l}}^{(i)}, \boldsymbol{\varepsilon}_{\boldsymbol{nl}}^{(i)}$and $\boldsymbol{\varepsilon}_{\boldsymbol{I}}^{(i)}$are respectively linear and nonlinear strain vectors and strain vector for initial geometric imperfection for $(i)^{th}$ sub-plate. Also, the vectors $\boldsymbol{\psi}^{(i)}$ and $\boldsymbol{\varepsilon}_{\boldsymbol{s}}^{(i)}$ are curvature and shear strains vectors, respectively, and they can be defined as

$$\boldsymbol{\varepsilon}_{\boldsymbol{l}}^{(i)} = \begin{Bmatrix} \dfrac{\partial u^{(i)}}{\partial x} \\ \dfrac{\partial v^{(i)}}{\partial y} \\ \dfrac{\partial u^{(i)}}{\partial y} + \dfrac{\partial v^{(i)}}{\partial x} \end{Bmatrix}, \quad \boldsymbol{\varepsilon}_{\boldsymbol{nl}}^{(i)} = \begin{Bmatrix} \dfrac{1}{2}\left(\dfrac{\partial w^{(i)}}{\partial x}\right)^2 \\ \dfrac{1}{2}\left(\dfrac{\partial w^{(i)}}{\partial y}\right)^2 \\ \dfrac{\partial w^{(i)}}{\partial x}\dfrac{\partial w^{(i)}}{\partial y} \end{Bmatrix},$$
$$\boldsymbol{\varepsilon}_{\boldsymbol{I}}^{(i)} = \begin{Bmatrix} \dfrac{\partial w^{(i)}}{\partial x}\dfrac{\partial w_I^{(i)}}{\partial x} \\ \dfrac{\partial w^{(i)}}{\partial y}\dfrac{\partial w_I^{(i)}}{\partial y} \\ \dfrac{\partial w^{(i)}}{\partial x}\dfrac{\partial w_I^{(i)}}{\partial y} + \dfrac{\partial w^{(i)}}{\partial y}\dfrac{\partial w_I^{(i)}}{\partial x} \end{Bmatrix} \tag{8}$$

And

$$\boldsymbol{\psi}^{(i)} = \begin{Bmatrix} \dfrac{\partial \varphi_x^{(i)}}{\partial x} \\ \dfrac{\partial \varphi_y^{(i)}}{\partial y} \\ \dfrac{\partial \varphi_x^{(i)}}{\partial y} + \dfrac{\partial \varphi_y^{(i)}}{\partial x} \end{Bmatrix}, \boldsymbol{\varepsilon}_{\boldsymbol{s}}^{(i)} = \begin{Bmatrix} \varphi_y^{(i)} + \dfrac{\partial w^{(i)}}{\partial y} \\ \varphi_x^{(i)} + \dfrac{\partial w^{(i)}}{\partial x} \end{Bmatrix} \tag{9}$$

With the assumption that each layer is in a condition of plane stress, stress-strain relationships for each lamina at a general point and for each sub-plate are written as below

$$\boldsymbol{\sigma}^{(i)} = \begin{Bmatrix} \sigma_{xx}^{(i)} \\ \sigma_{yy}^{(i)} \\ \tau_{xy}^{(i)} \end{Bmatrix} = \begin{bmatrix} \bar{Q}_{11} & \bar{Q}_{12} & \bar{Q}_{16} \\ \bar{Q}_{12} & \bar{Q}_{22} & \bar{Q}_{26} \\ \bar{Q}_{16} & \bar{Q}_{26} & \bar{Q}_{66} \end{bmatrix}^{(i)} \begin{Bmatrix} \bar{\varepsilon}_{xx}^{(i)} \\ \bar{\varepsilon}_{yy}^{(i)} \\ \bar{\varepsilon}_{xy}^{(i)} \end{Bmatrix} = \bar{\boldsymbol{Q}}^{(i)}\bar{\boldsymbol{\varepsilon}}^{(i)} \tag{10}$$

$$\boldsymbol{\sigma}_{\boldsymbol{s}}^{(i)} = \begin{bmatrix} \bar{Q}_{44} & \bar{Q}_{45} \\ \bar{Q}_{45} & \bar{Q}_{55} \end{bmatrix}^{(i)} \begin{Bmatrix} \varphi_y^{(i)} + \dfrac{\partial w^{(i)}}{\partial y} \\ \varphi_x^{(i)} + \dfrac{\partial w^{(i)}}{\partial x} \end{Bmatrix} = \bar{\boldsymbol{Q}}_{\boldsymbol{s}}^{(i)}\boldsymbol{\varepsilon}_{\boldsymbol{s}}^{(i)} \tag{11}$$

Where$\bar{\boldsymbol{Q}}^{(i)}$is transformed reduced stiffness matrix and $\bar{\boldsymbol{Q}}_{\boldsymbol{s}}^{(i)}$ is transformed shear stiffness matrix for $(i)^{th}$ sub-plate. Each composite sub-plate has its stiffness matrices $\boldsymbol{A}^{(i)}, \boldsymbol{B}^{(i)}, \boldsymbol{D}^{(i)}, \boldsymbol{A}_{\boldsymbol{s}}^{(i)}$that their coefficients can be obtained by

$$\left(\boldsymbol{A}_{pq}^{(i)}, \boldsymbol{B}_{pq}^{(i)}, \boldsymbol{D}_{pq}^{(i)}\right) = \int_{-h/2}^{h/2} \bar{\boldsymbol{Q}}_{pq}^{(i)}\,(1, z, z^2)dz, \ \ p, q = 1,2,3 \tag{12}$$

$$\boldsymbol{A}_{\boldsymbol{s}_{pq}}^{(i)} = k_s \int_{-h/2}^{h/2} \bar{\boldsymbol{Q}}_{\boldsymbol{s}_{pq}}^{(i)}\,dz, \ \ p, q = 1,2 \tag{13}$$

where k_s is the shear correction factor and it is assumed to be equal to 5/6 in this study. With the above definitions, the total potential energy of $(i)^{th}$ sub-plate can be obtained. At first, the strain energy associated with the in-plane stresses for $(i)^{th}$ sub-plate with volume $V^{(i)}$and surface area $\Omega^{(i)}$and by using the Eqs. (7) and (10) can be written as

$$\begin{aligned} U^{(i)} &= \frac{1}{2}\iiint_{V^{(i)}} \bar{\boldsymbol{\varepsilon}}^{(i)^T}\boldsymbol{\sigma}^{(i)}\mathrm{d}V^{(i)} \\ &= \frac{1}{2}\iint_{\Omega^{(i)}}\int_{-h/2}^{-h/2} \bar{\boldsymbol{\varepsilon}}^{(i)^T}\bar{\boldsymbol{Q}}^{(i)}\bar{\boldsymbol{\varepsilon}}^{(i)}\mathrm{d}z\,\mathrm{d}\Omega^{(i)} \\ &= \frac{1}{2}\iint_{\Omega^{(i)}}\int_{-h/2}^{-h/2} \left(\boldsymbol{\varepsilon}_{\boldsymbol{l}}^{(i)} + \boldsymbol{\varepsilon}_{\boldsymbol{nl}}^{(i)} + \boldsymbol{\varepsilon}_{\boldsymbol{I}}^{(i)} + z\boldsymbol{\psi}^{(i)}\right)^T \bar{\boldsymbol{Q}}^{(i)}\left(\boldsymbol{\varepsilon}_{\boldsymbol{l}}^{(i)} + \boldsymbol{\varepsilon}_{\boldsymbol{nl}}^{(i)} + \boldsymbol{\varepsilon}_{\boldsymbol{I}}^{(i)} + z\boldsymbol{\psi}^{(i)}\right)\mathrm{d}z\,\mathrm{d}\Omega^{(i)} \end{aligned} \tag{14}$$

By integrating through the thickness with respect to z from the Eq. (14) and substituting Eqs. (12) into Eq. (14), the strain energy can be rewritten as

$$U^{(i)} = \iint_{\Omega^{(i)}} \Big(\frac{1}{2} \boldsymbol{\varepsilon}_{l}^{(i)^T} \boldsymbol{A}^{(i)} \boldsymbol{\varepsilon}_{l}^{(i)} + \boldsymbol{\varepsilon}_{l}^{(i)^T} \boldsymbol{A}^{(i)} \boldsymbol{\varepsilon}_{nl}^{(i)} + \frac{1}{2} \boldsymbol{\varepsilon}_{nl}^{(i)^T} \boldsymbol{A}^{(i)} \boldsymbol{\varepsilon}_{nl}^{(i)} + \boldsymbol{\varepsilon}_{l}^{(i)^T} \boldsymbol{A}^{(i)} \boldsymbol{\varepsilon}_{I}^{(i)} + \boldsymbol{\varepsilon}_{nl}^{(i)^T} \boldsymbol{A}^{(i)} \boldsymbol{\varepsilon}_{I}^{(i)} + \frac{1}{2} \boldsymbol{\varepsilon}_{I}^{(i)^T} \boldsymbol{A}^{(i)} \boldsymbol{\varepsilon}_{I}^{(i)} + \boldsymbol{\psi}^{(i)^T} \boldsymbol{B}^{(i)} \boldsymbol{\varepsilon}_{I}^{(i)} + \boldsymbol{\varepsilon}_{l}^{(i)^T} \boldsymbol{B}^{(i)} \boldsymbol{\psi}^{(i)} + \boldsymbol{\varepsilon}_{nl}^{(i)^T} \boldsymbol{B}^{(i)} \boldsymbol{\psi}^{(i)} + \frac{1}{2} \boldsymbol{\psi}^{(i)^T} \boldsymbol{D}^{(i)} \boldsymbol{\psi}^{(i)} \Big) \mathrm{d}\Omega^{(i)}, i = 1, \ldots, 6 \tag{15}$$

In the next step, shear strain energy U_s for $(i)^{th}$ sub-plateshould be computed. It can be obtained by the following relation and by using the Eqs. (9), (11) and (13).

$$U_s^{(i)} = \frac{1}{2} \iiint_{V^{(i)}} \boldsymbol{\varepsilon}_{s}^{(i)^T} \boldsymbol{\sigma}_{s}^{(i)} \mathrm{d}V^{(i)} = \frac{1}{2} \iint_{\Omega^{(i)}} \int_{-h/2}^{-h/2} \boldsymbol{\varepsilon}_{s}^{(i)^T} \overline{\boldsymbol{Q}}_{s}^{(i)} \boldsymbol{\varepsilon}_{s}^{(i)} \mathrm{d}z \, \mathrm{d}\Omega^{(i)} = \frac{1}{2} \iint_{\Omega^{(i)}} \left(\boldsymbol{\varepsilon}_{s}^{(i)^T} \boldsymbol{A}_{s}^{(i)} \boldsymbol{\varepsilon}_{s}^{(i)} \right) \mathrm{d}\Omega^{(i)}, i = 1, \ldots, 6 \tag{16}$$

With regard to the above relations, the total strain energy of the plate can be computed by the summation of the strain energies of sub-plates. In order to calculate the total potential energy of the cracked plates in this study, it is also required to compute the potential energy of the applied loads. Therefore, the type of sub-plates layout (arrangement A or B) is very important, since some sub-plates may not be subjected directly to the applied load. In other words, the potential energy of applied loads for whole plate is affected by the loads applied on the external boundaries of the plate only. The potential energy of the applied loads for $(i)^{th}$ sub-plate in both arrangements A and B can be obtained by the following relations.

For arrangement A with applied loadP_x

$$V^{(i)} = \begin{cases} \frac{b^{(i)}}{B} P_x u^{(i)} \big|_{x=-a^{(i)}/2} & i = 1,3,5 \\ -\frac{b^{(i)}}{B} P_x u^{(i)} \big|_{x=a^{(i)}/2} & i = 2,4,6 \end{cases} \tag{17a}$$

For arrangement A with applied load P_y

$$V^{(i)} = \begin{cases} \frac{a^{(i)}}{A} P_y v^{(i)} \big|_{y=-b^{(i)}/2} & i = 1,2 \\ -\frac{a^{(i)}}{A} P_y v^{(i)} \big|_{y=b^{(i)}/2} & i = 5,6 \\ 0 & i = 3,4 \end{cases} \tag{17b}$$

For arrangement B with applied load P_x

$$V^{(i)} = \begin{cases} \frac{b^{(i)}}{B} P_x u^{(i)} \big|_{x=-a^{(i)}/2} & i = 1,4 \\ -\frac{b^{(i)}}{B} P_x u^{(i)} \big|_{x=a^{(i)}/2} & i = 3,6 \\ 0 & i = 2,5 \end{cases} \tag{17c}$$

As a result, the total potential energy for each sub-plate is equal to the summation of the strain energies of that sub-plate with the potential energy of the applied load $V^{(i)}$. The total potential energy of the cracked laminated plates can also be computed by the summation of the total potential energies of the sub-plates. However, since the entire domain of the laminates in this study has been partitioned into several sub-plates using the plate decomposition technique, therefore the interface continuity between the sub-plates should be enforced wherever it is needed. Actually, the displacement continuity conditions for different types of sub-plates layout (arrangement A or B) read as

For arrangement A

$$\begin{aligned} \tau^{(1)}\big(a^{(1)}/2, y\big) &= \tau^{(2)}\big(-a^{(2)}/2, y\big) \\ \tau^{(1)}\big(x, b^{(1)}/2\big) &= \tau^{(3)}\big(x, -b^{(3)}/2\big) \\ \tau^{(2)}\big(x, b^{(2)}/2\big) &= \tau^{(4)}\big(x, -b^{(4)}/2\big) \\ \tau^{(3)}\big(x, b^{(3)}/2\big) &= \tau^{(5)}\big(x, -b^{(5)}/2\big) \\ \tau^{(4)}\big(x, b^{(4)}/2\big) &= \tau^{(6)}\big(x, -b^{(6)}/2\big) \\ \tau^{(5)}\big(a^{(5)}/2, y\big) &= \tau^{(6)}\big(-a^{(6)}/2, y\big) \end{aligned} \tag{18a}$$

Where$\tau \in \{u, v, w, \varphi_x, \varphi_y\}$ and for arrangement B

$$\begin{aligned} \tau^{(1)}\big(a^{(1)}/2, y\big) &= \tau^{(2)}\big(-a^{(2)}/2, y\big) \\ \tau^{(1)}\big(x, b^{(1)}/2\big) &= \tau^{(4)}\big(x, -b^{(4)}/2\big) \\ \tau^{(2)}\big(a^{(2)}/2, y\big) &= \tau^{(3)}\big(-a^{(3)}/2, y\big) \\ \tau^{(3)}\big(x, b^{(3)}/2\big) &= \tau^{(6)}\big(x, -b^{(6)}/2\big) \\ \tau^{(4)}\big(a^{(4)}/2, y\big) &= \tau^{(5)}\big(-a^{(5)}/2, y\big) \\ \tau^{(5)}\big(a^{(5)}/2, y\big) &= \tau^{(6)}\big(-a^{(6)}/2, y\big) \end{aligned} \tag{18b}$$

As it can be seen, for arrangement A, sub-plates 3 and 4 have no connection to each other to accurately model the crack in the plate as well as sub-plates 2 and 5 for arrangement B. As mentioned before, penalty technique is used here to enforce displacement continuity along the edges shared between the sub-plates. Therefore, the equilibrium equations of the cracked plate are obtained by imposing the stationary of total potential energy under the constraints presented in Eq. (18). The enforcement of these constraints is accomplished by introducing the following penalty terms into the total potential energy functional.

For arrangement A, the penalty terms associated with Eqs. (18a) can be obtained by

$$\begin{aligned} P_{1,2}^{\langle\tau\rangle} &= \frac{\gamma_{1,2}^{\langle\tau\rangle}}{2} \int_{-b^{(1)}/2}^{b^{(1)}/2} \Big(\tau^{(1)}\big(a^{(1)}/2, y\big) - \tau^{(2)}\big(-a^{(2)}/2, y\big)\Big)^2 \mathrm{d}y \\ P_{1,3}^{\langle\tau\rangle} &= \frac{\gamma_{1,3}^{\langle\tau\rangle}}{2} \int_{-a^{(1)}/2}^{a^{(1)}/2} \Big(\tau^{(1)}\big(x, b^{(1)}/2\big) - \tau^{(3)}\big(x, -b^{(3)}/2\big)\Big)^2 \mathrm{d}x \end{aligned} \tag{19}$$

$$P_{2,4}^{\langle\tau\rangle}=\frac{\gamma_{2,4}^{\langle\tau\rangle}}{2}\int_{-a^{(2)}/2}^{a^{(2)}/2}\left(\tau^{(2)}\left(x,b^{(2)}/2\right)-\tau^{(4)}\left(x,-b^{(4)}/2\right)\right)^2\mathrm{d}x$$

$$P_{3,5}^{\langle\tau\rangle}=\frac{\gamma_{3,5}^{\langle\tau\rangle}}{2}\int_{-a^{(3)}/2}^{a^{(3)}/2}\left(\tau^{(3)}\left(x,b^{(3)}/2\right)-\tau^{(5)}\left(x,-b^{(5)}/2\right)\right)^2\mathrm{d}x$$

$$P_{4,6}^{\langle\tau\rangle}=\frac{\gamma_{4,6}^{\langle\tau\rangle}}{2}\int_{-a^{(4)}/2}^{a^{(4)}/2}\left(\tau^{(4)}\left(x,b^{(4)}/2\right)-\tau^{(6)}\left(x,-b^{(6)}/2\right)\right)^2\mathrm{d}x$$

$$P_{5,6}^{\langle\tau\rangle}=\frac{\gamma_{5,6}^{\langle\tau\rangle}}{2}\int_{-b^{(5)}/2}^{b^{(5)}/2}\left(\tau^{(5)}\left(a^{(5)}/2,y\right)-\tau^{(6)}\left(-a^{(6)}/2,y\right)\right)^2\mathrm{d}y$$

Where $\tau\in\{u,v,w,\varphi_x,\varphi_y\}$ and γ are penalty coefficients. Finally, a single relation can be written for the penalty terms.

$$P=\sum_{\tau\in\{u,v,w,\varphi_x,\varphi_y\}}\left(P_{1,2}^{\langle\tau\rangle}+P_{1,3}^{\langle\tau\rangle}+P_{2,4}^{\langle\tau\rangle}+P_{3,5}^{\langle\tau\rangle}+P_{4,6}^{\langle\tau\rangle}+P_{5,6}^{\langle\tau\rangle}\right)\tag{20}$$

The same relations can be written for arrangement B.

With the above descriptions, the total potential energy of a cracked plate is equal to the summation of the strain energies of the sub-plates (i.e., Eqs. (15) and (16)) with potential energies of the applied load for sub-plates (i.e., Eq. (17)) and penalty terms associated with constraints presented in Eq. (18).

$$\Pi=\sum_{i=1}^{6}\left(U^{(i)}+U_s^{(i)}+V^{(i)}\right)+P\tag{21}$$

By using the Eqs. (15) and (16), the total potential energy of the cracked laminate can be rewritten in an appropriate category as follows.

$$\begin{aligned}\Pi&=\sum_{i=1}^{6}V^{(i)}\\&+\Bigg\{P+\sum_{i=1}^{6}\Bigg(\iint_{\Omega^{(i)}}\Big(\frac{1}{2}\boldsymbol{\varepsilon}_l^{(i)T}\boldsymbol{A}^{(i)}\boldsymbol{\varepsilon}_l^{(i)}+\frac{1}{2}\boldsymbol{\psi}^{(i)T}\boldsymbol{D}^{(i)}\boldsymbol{\psi}^{(i)}\\&+\boldsymbol{\varepsilon}_l^{(i)T}\boldsymbol{B}^{(i)}\boldsymbol{\psi}^{(i)}+\frac{1}{2}\boldsymbol{\varepsilon}_s^{(i)T}\boldsymbol{A}_s^{(i)}\boldsymbol{\varepsilon}_s^{(i)}+\boldsymbol{\varepsilon}_l^{(i)T}\boldsymbol{A}^{(i)}\boldsymbol{\varepsilon}_I^{(i)}\\&+\frac{1}{2}\boldsymbol{\varepsilon}_I^{(i)T}\boldsymbol{A}^{(i)}\boldsymbol{\varepsilon}_I^{(i)}+\boldsymbol{\psi}^{(i)T}\boldsymbol{B}^{(i)}\boldsymbol{\varepsilon}_I^{(i)}\Big)\mathrm{d}\Omega^{(i)}\Bigg)\Bigg\}\\&+\sum_{i=1}^{6}\Bigg(\iint_{\Omega^{(i)}}\Big(\boldsymbol{\varepsilon}_l^{(i)T}\boldsymbol{A}^{(i)}\boldsymbol{\varepsilon}_{nl}^{(i)}+\boldsymbol{\varepsilon}_{nl}^{(i)T}\boldsymbol{B}^{(i)}\boldsymbol{\psi}^{(i)}\\&+\boldsymbol{\varepsilon}_{nl}^{(i)T}\boldsymbol{A}^{(i)}\boldsymbol{\varepsilon}_I^{(i)}\Big)\mathrm{d}\Omega^{(i)}\Bigg)\\&+\sum_{i=1}^{6}\Bigg(\iint_{\Omega^{(i)}}\Big(\frac{1}{2}\boldsymbol{\varepsilon}_{nl}^{(i)T}\boldsymbol{A}^{(i)}\boldsymbol{\varepsilon}_{nl}^{(i)}\Big)\mathrm{d}\Omega^{(i)}\Bigg)\end{aligned}\tag{22}$$

By looking at the above expression, it is easy to see that there is a clear division. The first term in the right-hand side of the above equation is linear function of the unknowns while the rest of the terms is quadratic, cubic and quartic functions of the unknowns, respectively. The linear term arises from the potential energy of applied loads. The quadratic energy comprises contributions from the linear strain vector, from the curvature strain vector, from coupling between these two vectors due to the material effects (i.e. $\boldsymbol{B}$ matrix), from shear strain vector and from initial imperfection effects. The cubic energy originates from coupling between linear and nonlinear strain vectors, from coupling between curvature and nonlinear strain vectors again due to material effects and also from initial imperfection effects. The quartic energy arises from the nonlinear strain vectors alone.

The above equation can ultimately be rewritten in a matrix form by using the Hessian technique.

$$\begin{aligned}\Pi=-\boldsymbol{d}^T\boldsymbol{V}_F+\frac{1}{2}\boldsymbol{d}^T(\boldsymbol{K}_{0P}+\boldsymbol{K}_0+\boldsymbol{K}_{0s}+\boldsymbol{K}_{0I})\boldsymbol{d}\\+\frac{1}{6}\boldsymbol{d}^T(\boldsymbol{K}_1+\boldsymbol{K}_{1I})\boldsymbol{d}+\frac{1}{12}\boldsymbol{d}^T\boldsymbol{K}_2\boldsymbol{d}\end{aligned}\tag{23}$$

where $\boldsymbol{V}_F$ is a column matrix of constants, including the effects of the applied loads. The column matrix $\boldsymbol{d}$ contains the unknown of the problems. Subscripts P and I denote the effects of penalty terms and initial imperfection, respectively. Subscript 0 is for symmetric square stiffness matrices whose coefficients are constant whilst subscript 1 and 2 are for matrices with linear and quadratic functions of the unknown coefficients, respectively. Therefore, the quantities on the right-hand side of the Eq. (23) represent linear, quadratic and cubic energy terms. Solution of the nonlinear problem is sought through the application of the Principle of Minimum Potential Energy. Therefore, the unknown coefficients of the problem can be found by solving the following nonlinear equilibrium equations

$$\begin{aligned}\boldsymbol{F}(\boldsymbol{d})=-\boldsymbol{V}_F+\Big((\boldsymbol{K}_{0P}+\boldsymbol{K}_0+\boldsymbol{K}_{0s}+\boldsymbol{K}_{0I})\\+\frac{1}{2}(\boldsymbol{K}_1+\boldsymbol{K}_{1I})+\frac{1}{3}\boldsymbol{K}_2\Big)\boldsymbol{d}=\boldsymbol{0}\end{aligned}\tag{24}$$

To obtain the solution of the above nonlinear algebraic equations, the well-known Newton-Raphson technique is used. In this study, in order to obtain the accurate results, the relevant convergence criteria are defined based on both the vector containing the unknown coefficients ($\boldsymbol{d}$) and all equations containing these coefficients i.e., $\boldsymbol{F}(\boldsymbol{d})$. The iterative procedure is repeated until the following conditions be satisfied.

$$\frac{\|\Delta\boldsymbol{d}_r\|}{\|\boldsymbol{d}_{r+1}\|}<5\times10^{-5},\qquad\|\boldsymbol{F}(\boldsymbol{d}_r)\|<5\times10^{-5}\tag{25}$$

where r is the iteration counter in Newton-Raphson technique and $\|.\|$ denotes the 2-norm. Once the nonlinear equilibrium equations are solved and the unknown coefficients are found, it is possible to calculate the displacements, strains and stresses at any point in the cracked plate.

4. Results and discussions

In this section, in order to implement the presented formulations for analyzing the nonlinear behavior of internally and edge cracked composite plates, a computer program is developed based on Fortran 77 software package. To reduce the execution time on multicore processors, a parallel programming technique is used using Open Multi-Processing (OpenMP) interface. The program is executed on a computer with TYAN FT48-B8812 mainboard, four AMD CPU by 2.20 GHz frequency (4×16 cores) and with 128.00 GB RAM.

The presented formulations should be verified through a number of comparisons and this is done by comparing the results with those obtained by ABAQUS software. Wherever the results are compared with finite element method, S4R shell element has been used. To obtain converged results, in most cases, 2500 elements have been used.

To investigate the effects of boundary conditions on post-buckling behavior of cracked laminates, three different types of boundary conditions are assumed as follows:

• Type A: Simply supported boundary conditions on all edges.
• Type B: Two loaded edges simply supported and one unloaded edge clamped and the other simply supported.
• Type C: Two loaded edges simply supported and one unloaded edge clamped and the other free.

In the extraction of the results, some sensitivity analyzes have been made with respect to the crack location and length. To do this, the crack is considered to be located at three different distances from the one side ($x_c = A/4, 3A/8, A/2$) and in each of these locations, four different lengths of crack are assumed($L_c = A/5, A/3, A/2, 2A/3$). To investigate the effects of loading direction, as already mentioned, the plate is decomposed into two different configurations, and thus, the crack is placed either along the load direction or in the perpendicular direction (see Figure 2). To obtain the above results, square laminated plates ($A = B$) with thickness to length ratio (h/A) of 0.1 are considered in this study. The lay-up configuration for the laminates under consideration, is assumed to be$[0,90]_3$. Before presentation of the results, it is necessary to mention that in this study, no thinking has been done to simulate eventual contact between the crack faces. In other words, no contact interface has been defined between the sub-plates at the crack location. Therefore, for the cracked plates, especially when the crack is perpendicular to the loading direction, the crack faces may contact each other. But since the composite layup is assumed as unsymmetric, the possibility of occurrence of this phenomenon is reduced. However, it is avoided to present such results as far as possible.

The material properties for each lamina have been taken from Yang *et al.* (2013) and are shown in Table 1.

For imperfect laminates, an initial sinusoidal imperfection in both directions is assumed with amplitude of 10% and 50% of the plate thickness (i.e., $w_0 = 0.1h$ & $0.5h$).

In the first step, it is necessary to carry out the convergence study to calculate the appropriate number of terms for obtaining accurate results. For this purpose, an internally cracked plate with boundary conditions type A is considered. In order to place the crack orthogonal to the loading direction, plate decomposition configuration is selected to be arrangement A. The crack is considered to be placed at $x_c = 3A/8$ and the assumed length for the crack is $L_c = A/3$.

Table 1 Assumed material properties for each lamina

Component	Value
$E_1(MPa)$	49627
$E_2(MPa)$	15430
υ_{12}	0.272
$G_{12}(MPa)$	4800
$G_{13}(MPa)$	4800
$G_{23}(MPa)$	4800

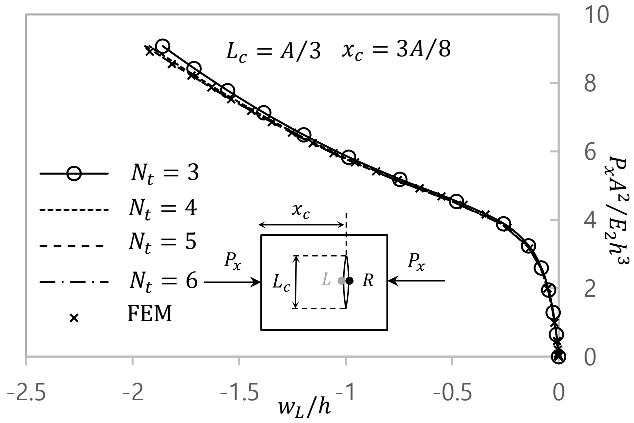

Fig. 4 Convergence study for internally cracked plate with boundary conditions type A and arrangement A

According to Fig. 4, which indicates the variation of force in terms of out-of-plane displacement, the convergent results are obtained by taking into account the 25 terms in series expansion of each displacement field ($N_t = 5$) and for each sub-plate. In the case of imperfect cracked plates, for the sake of confidence, the results are calculated by 36 terms ($N_t = 6$). As shown in this figure, the results obtained by the finite element method are also incorporated in order to validate the results. An excellent agreement between the results can be observed.

Variations of load in terms of both in-plane and out-of-plane displacements are depicted in Figs. 5-12. In these figures, the effects of crack length and location have been investigated for laminates with all simply-supported edges (boundary condition type A). The crack in these laminates have been modeled by plate decomposition arrangement A.

The laminates have been subjected to in-plane compressive load P_x along the x-direction and therefore the crack axis is orthogonal to the applied load direction. According to the observations, when the crack length is greater than$A/2$ ($L_c > A/2$), crack opening does not occur. In Figs. 5 and 6, the crack has been placed at the middle of

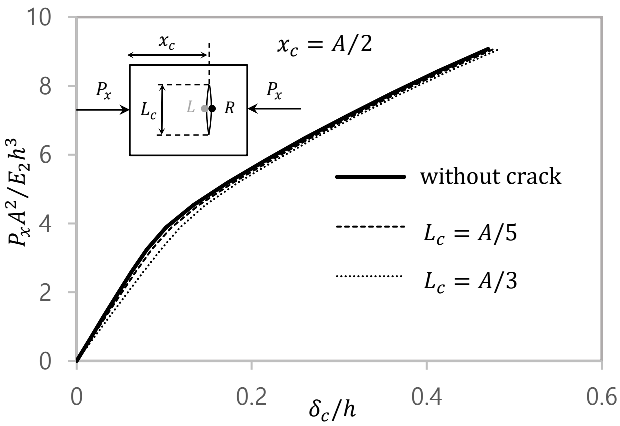

Fig. 5 Variations of load versus end shortening displacement for plates subjected to P_x with different lengths of crack (type A, arrangement A, $x_c = A/2$)

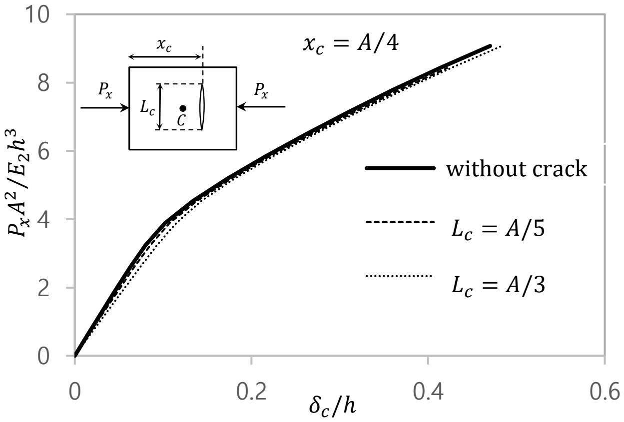

Fig. 7 Variations of load versus end shortening displacement for plates subjected to P_x with different lengths of crack (type A, arrangement A, $x_c = A/4$)

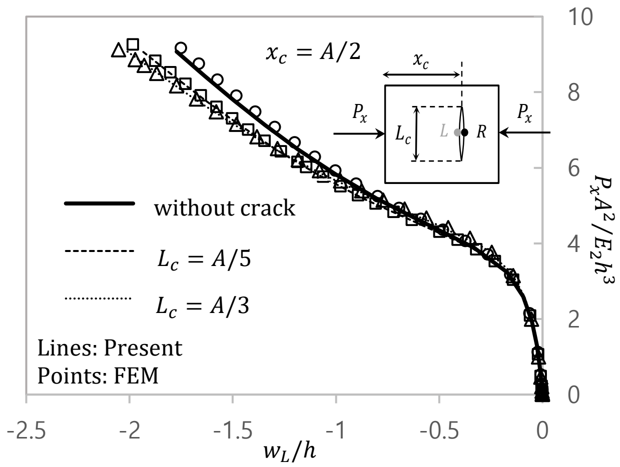

Fig. 6 Variations of load versus out-of-plane displacement for plates subjected to P_x with different lengths of crack (type A, arrangement A, $x_c = A/2$)

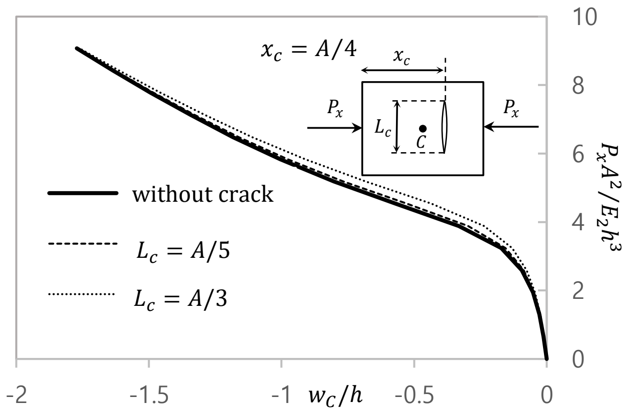

Fig. 8 Variations of load versus out-of-plane displacement for plates subjected to P_x with different lengths of crack (type A, arrangement A, $x_c = A/4$)

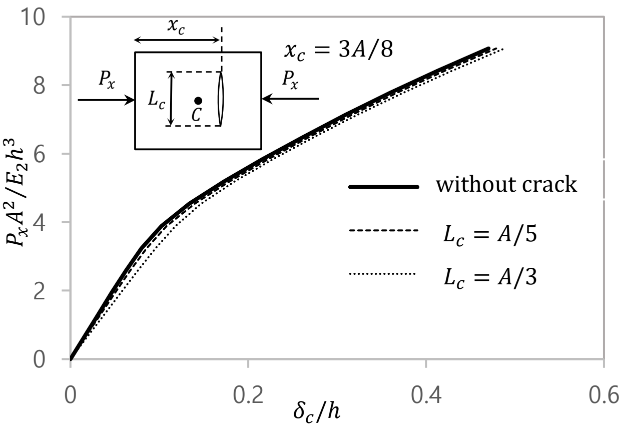

Fig. 9 Variations of load versus end shortening displacement for plates subjected to P_x with different lengths of crack (type A, arrangement A, $x_c = 3A/8$)

the plate $(x_c = A/2)$ while in Figs. 7 and 8, the location of the crack has been shifted to the left by $A/4$ $(x_c = A/4)$ and this shifted amount for Figs. 9 and 10 is$3A/8$ $(x_c = 3A/8)$. As it can be seen in these figures, by changing the crack length, the variations of load versus both in-plane and out-of-plane displacements are changed in such a way that by increasing the length of the crack, the slope of the curve of load versus in-plane displacement is reduced and therefore the stiffness of the laminate is also decreased. This happens especially during the early stages of loading while at higher level of loading, the results will be closer to each other (see Figs. 5, 7 and 9). It is also seen that by increasing the length of crack, the central out-of-plane displacement of the laminates in which the cracks are located at the center, are increased at the same level of loading and this increase is more evident at the higher level of loading (see Fig. 6) while in the laminates in which the cracks are shifted to the left (see Figs. 8 and 10), the central out-of-plane displacement of the laminates are slightly decreased. It is noted that some results obtained by finite element method have been also incorporated and displayed by points in these figures to show the verification of

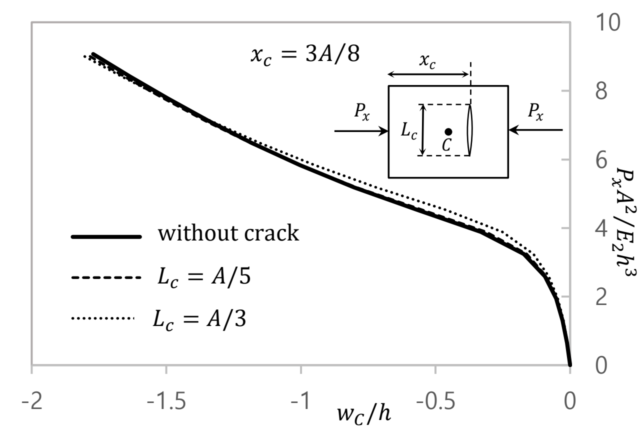

Fig. 10 Variations of load versus out-of-plane displacement for plates subjected to P_x with different lengths of crack (type A, arrangement A, $x_c = 3A/8$)

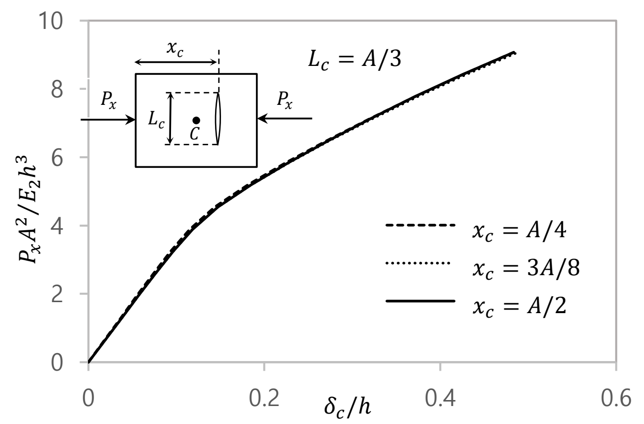

Fig. 11 Variations of load versus end shortening displacement for plates subjected to P_x with different locations of crack (type A, arrangement A, $L_c = A/3$)

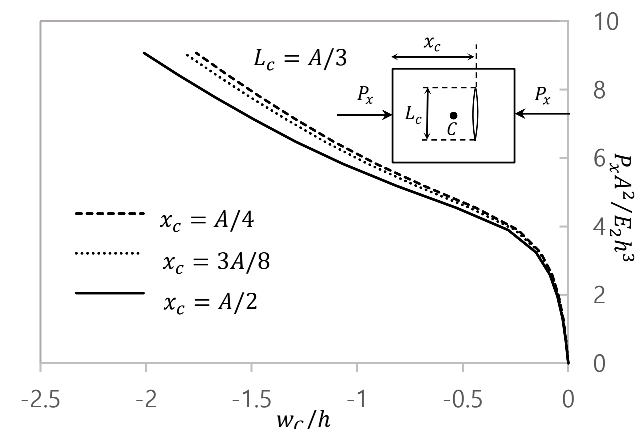

Fig. 12 Variations of load versus out-of-plane displacement for plates subjected to P_x with different locations of crack (type A, arrangement A, $L_c = A/3$)

proposed formulation.

Figs. 11 and 12 show the effect of various locations of crack from one edge of the plate for laminate with symmetric boundary conditions on all edges (type A) and for a specified length of crack (i.e., $L_c = A/3$). It has been observed that increasing the distance between the crack location and the middle of the plate leads to decreasing the out-of-plane displacement at the center of the plate.

Another purpose of the paper was to investigate the effects of cracks in the laminates with different boundary conditions. So, in this section, the type of boundary conditions is changed to boundary conditions type C. In this type of boundary conditions, with a free edge, the crack is placed at the free edge and so the possibility of investigating the edge crack is also provided. In this situation, the crack has been located perpendicularly to the loading direction P_x and therefore the decomposition configuration is arrangement A. Nonlinear behaviors of the laminates with this geometry, are represented in Figs. 13-20. In these figures, similar to the previous figures for type A, the effects of crack length and location have been investigated.

In addition to the considered lengths of the crack in the previous figures, the results for crack length of $A/2$ (i.e., $L_c = A/2$) have been added to the results of Figs. 13 to 18. As it can be seen, a similar behavior with Figs. 5, 7 and 9 is also observed in Figs. 13, 15 and 17 in which, increasing the length of the crack leads to a decrease in the curve slope, and thus the stiffness of the plates decreases but this behavior, with increasing the load is more visible in this type of boundary condition.

The nonlinear behaviors of load in terms of out-of-plane displacements for the laminates under consideration have been shown in Figs. 14, 16 and 18. In these figures, the central point of the free edge of the laminates has been marked by the letter “e” and the point on the right crack face on the free edge of the plate has been marked by the letter “R” in red color. Therefore, it is noted that in some figures containing red curves, they represent the out-of-plane displacement of the point on the right crack face on the free edge of the plate. It can be observed that by increasing the length of the cracks, the central out-of-plane displacement of the free edge of the laminates and also the displacement of the point on the right crack face on the free edge are almost increased at the same level of loading and this increase in the amount of displacement of points on right face of crack is much greater than the middle points of the free edge. However, a different behavior is seen for the case of cracks with length of $A/2$ especially at the early stages of loading.

To study the effects of different locations of edge cracks with a specified length (i.e., $L_c = A/2$), similar curves are depicted in Figs. 19 and 20. Looking at these figures, this concept is found that by moving the cracks from the middle of the free edge, the out-of-plane displacement of the middle of the free edge is significantly reduced.

In Fig. 20, three-dimensional deformation of these plates is also shown at a particular load $P_xA^2/E_2h^3 = 6$. The results of three-dimensional deformations have been plotted by the data extracted from the developed code and using Tecplot plotting software.

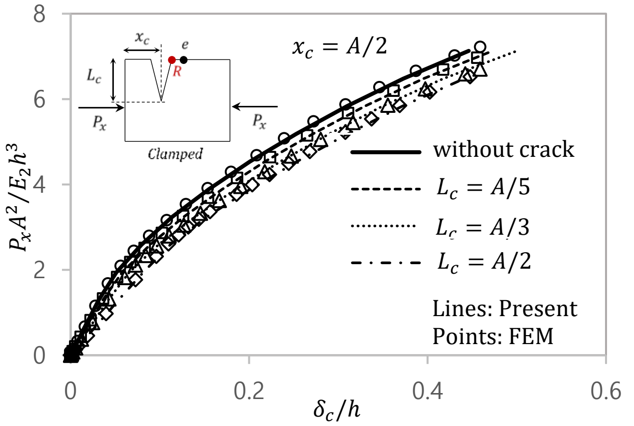

Fig. 13 Variations of load versus end shortening displacement for plates subjected to P_x with different lengths of crack (type C, arrangement A, $x_c = A/2$)

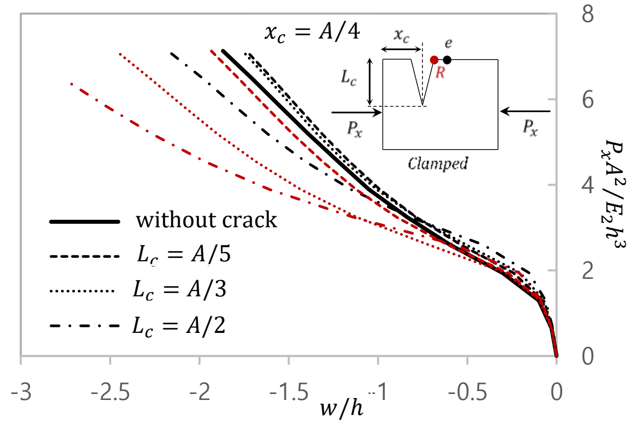

Fig. 16 Variations of load versus out-of-plane displacement for plates subjected to P_x with different lengths of crack (type C, arrangement A, $x_c = A/4$)

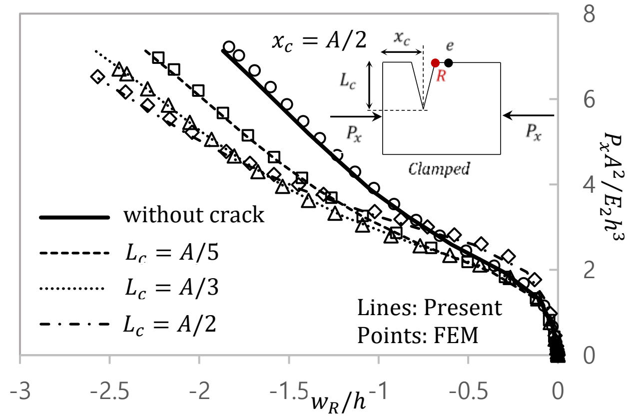

Fig. 14 Variations of load versus out-of-plane displacement for plates subjected to P_x with different lengths of crack (type C, arrangement A, $x_c = A/2$)

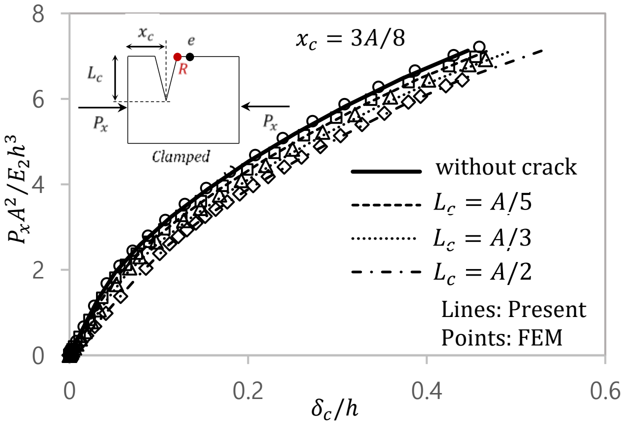

Fig. 17 Variations of load versus end shortening displacement for plates subjected to P_x with different lengths of crack (type C, arrangement A, $x_c = 3A/8$)

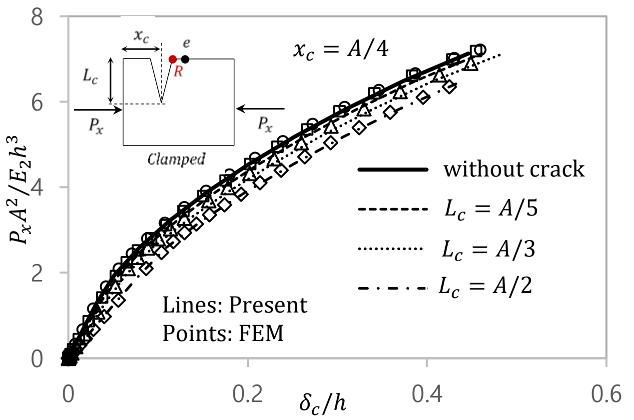

Fig. 15 Variations of load versus end shortening displacement for plates subjected to P_x with different lengths of crack (type C, arrangement A, $x_c = A/4$)

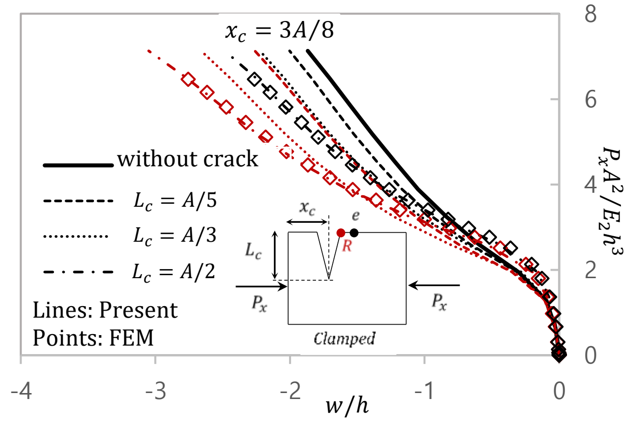

Fig. 18 Variations of load versus out-of-plane displacement for plates subjected to P_x with different lengths of crack (type C, arrangement A, $x_c = 3A/8$)

In the next step, the aim is to investigate the behavioral difference between the plates containing the cracks in both parallel and perpendicular to the loading direction. To implement this goal, some square laminates with boundary conditions type A and decomposition configuration of arrangement A are considered here. The laminates are

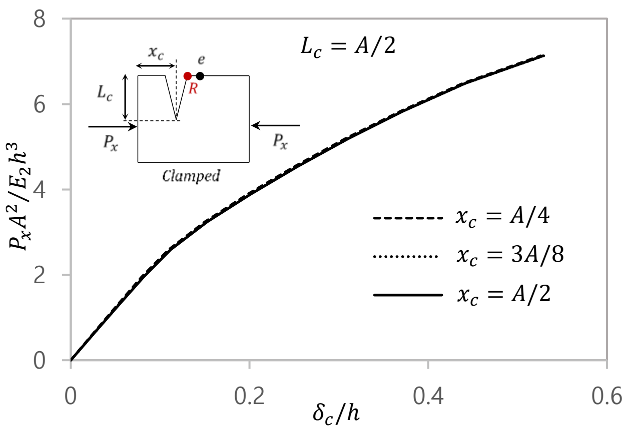

Fig. 19 Variations of load versus end shortening displacement for plates subjected to P_x with different locations of crack (type C, arrangement A, $L_c = A/2$)

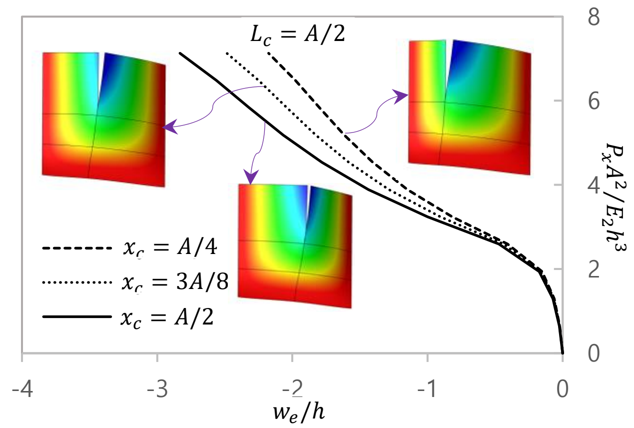

Fig. 20 Variations of load versus out-of-plane displacement for plates subjected to P_x with different locations of crack (type C, arrangement A, $L_c = A/2$)

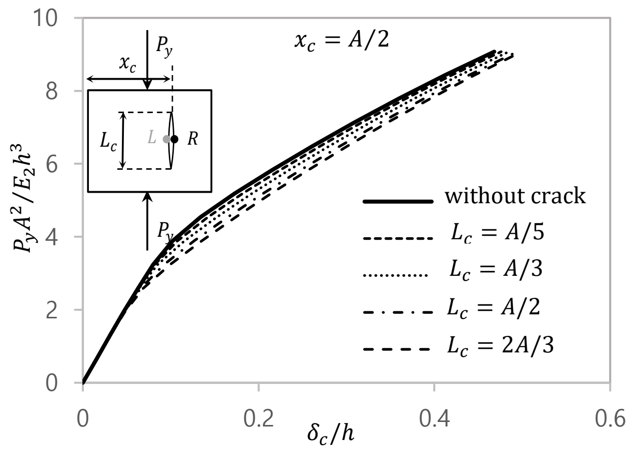

Fig. 21 Variations of load versus end shortening displacement for plates subjected to P_y with different lengths of crack (type A, arrangement A, $x_c = A/2$)

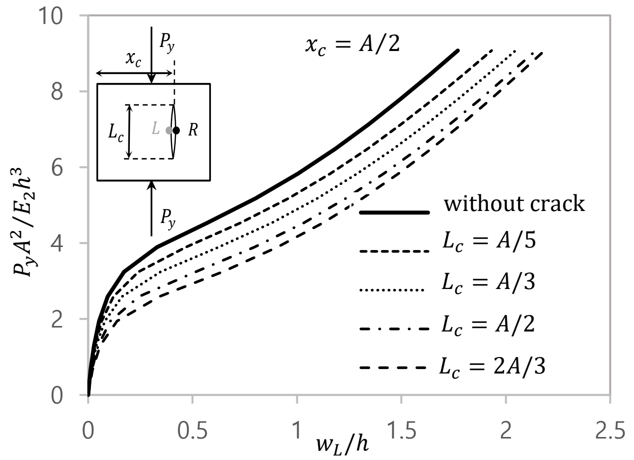

Fig. 22 Variations of load versus out-of-plane displacement for plates subjected to P_y with different lengths of crack (type A, arrangement A, $x_c = A/2$)

subjected to in-plane compressive load P_x along the x-direction or P_y along the y-direction.

Variations of load in terms of both in-plane and out-of-plane displacements are depicted in Figs. 21-28. According to observations, when the crack is along the loading direction, the crack opening is greater than the one in which the crack axis is perpendicular to the loading direction. Unlike the loading that its directionselected lengths of the crack in the situation where the loading direction is parallel to the crack axis (i.e., P_y along the y-direction) and therefore the graphs have been provided up to the crack length of $2A/3$. In Figs. 21-26, which are related to the plates containing the crack parallel to the loading direction, the same behaviors can be observed with the previous figures, but more intensely. As it is seen, in the longer cracks, the crack opening is greater and therefore the laminates are weaker. In Figs. 27 and 28, the results of both loadings P_x and P_y have been represented for laminates with and without crack. According to the Fig. 27, it is seen that the responses of the laminates without crack are the same for both loading due to symmetry, as is perpendicular to the crack (i.e., P_x along the x-direction), the crack opening is always observed at all expected. However, when there is a crack in the laminates, the results are completely different. In Fig. 28, in addition to representing the load variations in terms of out-of-plane displacements, deformation of these plates is also shown at a particular non-dimensional load factor of 9. As one can see, crack opening is more when the crack is along the direction of loading (the deformation specified by point point). The results of deformations have been plotted by the data extracted from the developed code and using Tecplot plotting software.

In another investigation, the boundary conditions type B in which one edge is clamped are used for laminates whose modeling is of arrangement B. As mentioned before, in this configuration, the laminates are subjected to in-plane compressive load P_x along the x-direction.

Since the effects of the change in the length of the cracks have already been observed in details for the plates

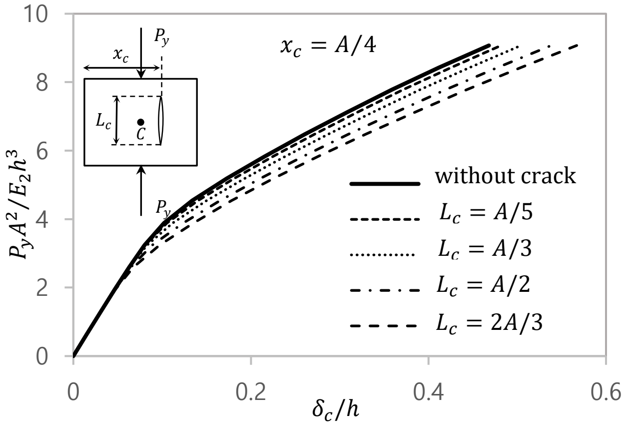

Fig. 23 Variations of load versus end shortening displacement for plates subjected to P_y with different lengths of crack (type A, arrangement A, $x_c = A/4$)

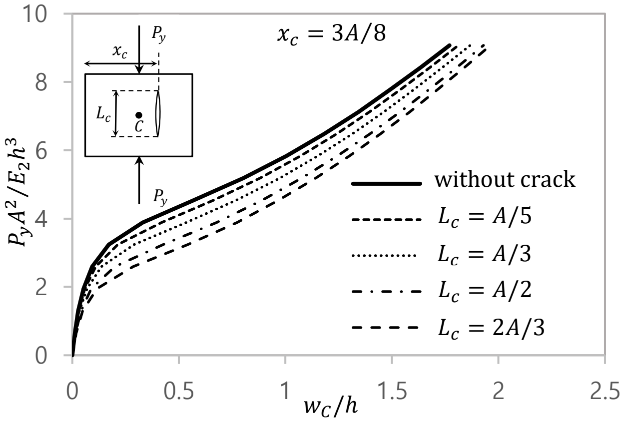

Fig. 26 Variations of load versus out-of-plane displacement for plates subjected to P_y with different lengths of crack (type A, arrangement A, $x_c = 3A/8$)

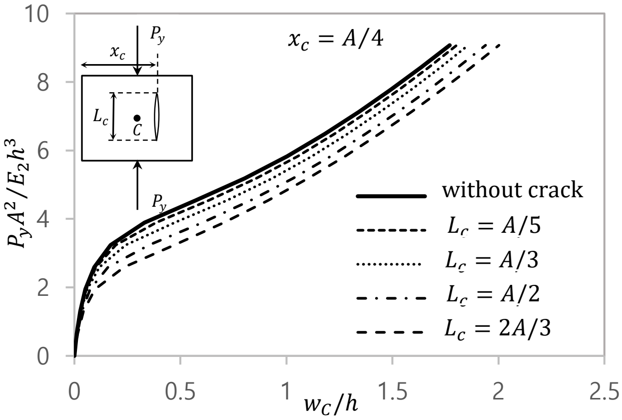

Fig. 24 Variations of load versus out-of-plane displacement for plates subjected to P_y with different lengths of crack (type A, arrangement A, $x_c = A/4$)

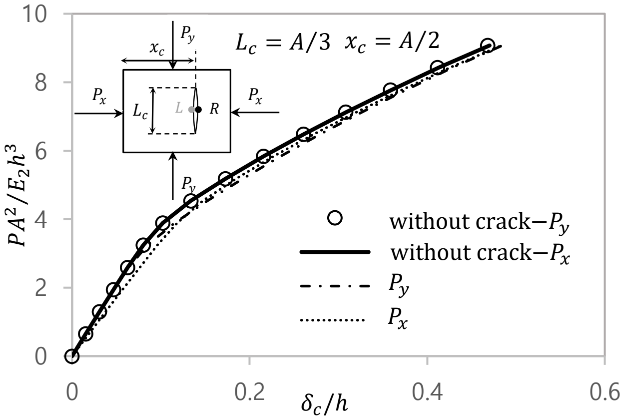

Fig. 27 Variations of load versus end shortening displacement for plates subjected to compressive loads with different directions (type A, arrangement A, $x_c = A/2$, $L_c = A/3$)

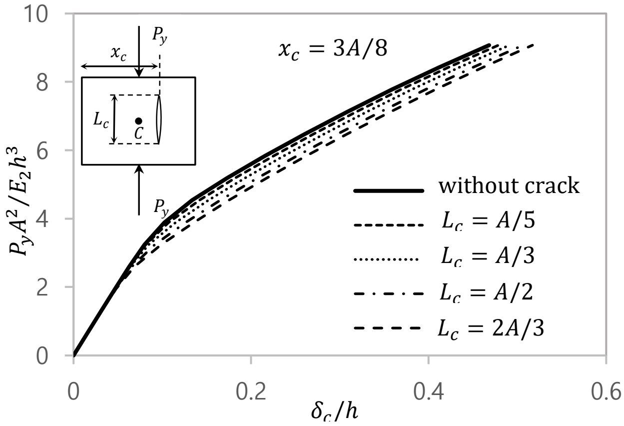

Fig. 25 Variations of load versus end shortening displacement for plates subjected to P_y with different lengths of crack (type A, arrangement A, $x_c = 3A/8$)

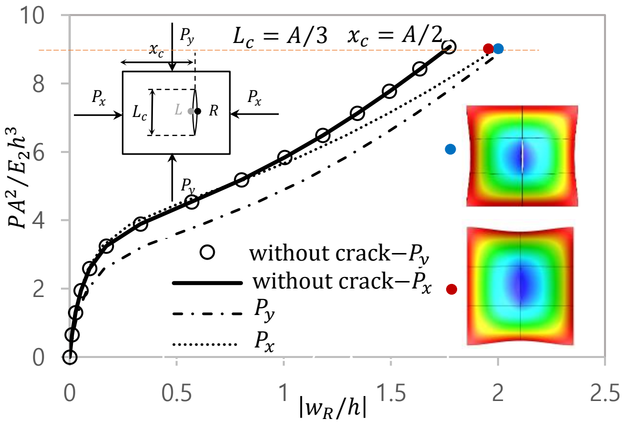

Fig. 28 Variations of load versus out-of-plane displacement for plates subjected to compressive loads with different directions (type A, arrangement A, $x_c = A/2$ $L_c = A/3$)

with boundary conditions type A and C, this will no longer be addressed in this type of boundary conditions (type B), and only the examination of the crack location relative to the clamped edge is made on these plates. Also, since the boundary conditions are non-symmetric along the y-direction, crack is modeled in more locations $y_c = A/4, 3A/8, A/2, 5A/8 \text{and} 3A/4$.

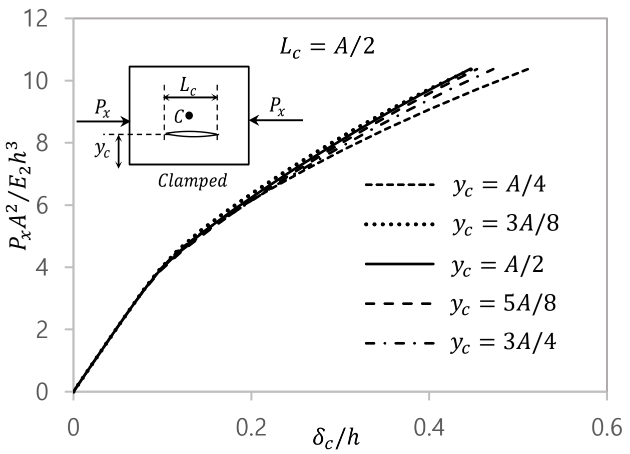

Fig. 29 Variations of load versus end shortening displacement for plates subjected to P_x with different locations of crack (type B, arrangement B, $L_c = A/2$)

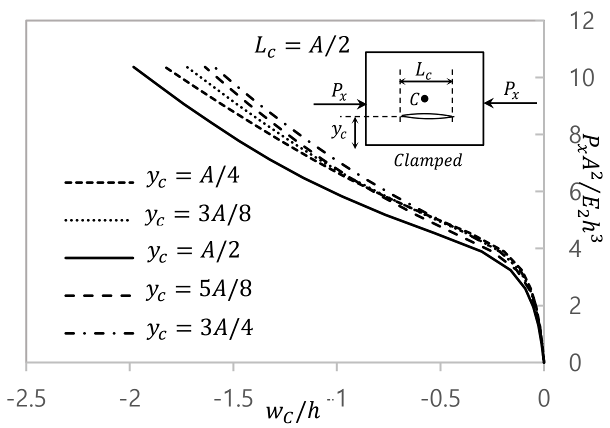

Fig. 30 Variations of load versus out-of-plane displacement for plates subjected to P_x with different locations of crack (type B, arrangement B, $L_c = A/2$)

The variations of loads versus end shortening displacement and central out-of-plane displacement of the plate have been depicted in Figs. 29 and 30 for a prescribed crack length$L_c = L/2$. As it can be observed, by changing the location of the crack and moving it away from the clamped edge, the response of the plate changes. It can be said that when the crack is in the closest location to the clamped edge, the stiffness of the cracked plate is decreased.

A comparison between the results of the laminates with both boundary conditions of types A and B is also made in Fig. 31. The crack has been modeled by using arrangement B and the laminates have been subjected to in-plane compressive load along the x-direction (P_x) and therefore the crack axis is parallel to the loading direction. To better observation, the three-dimensional deformation of these plates (plates containing crack) are also included in these figures.

In the last step, a comprehensive study has been done on the effects of crack length and location on nonlinear

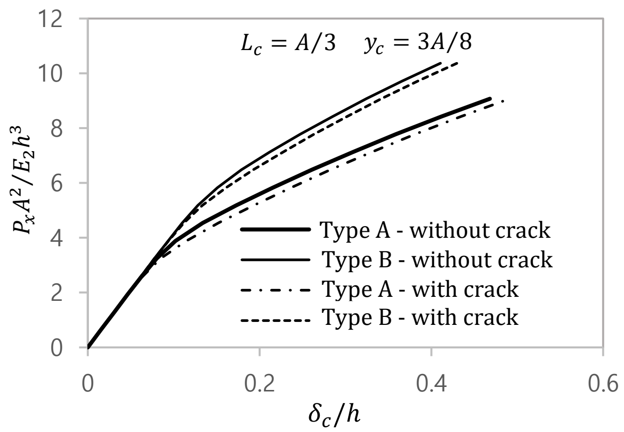

(a) Variation of load versus end shortening displacement

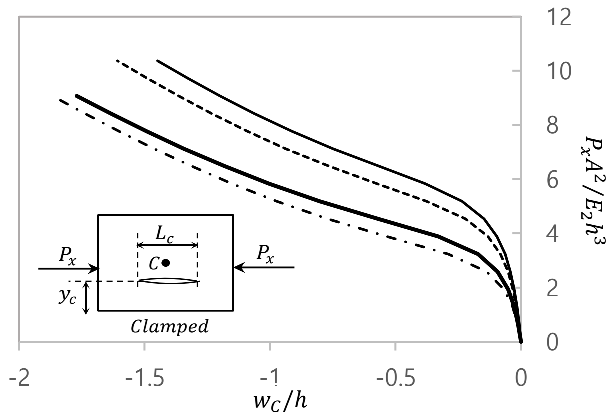

(b) Variation of load versus out-of-plane displacement

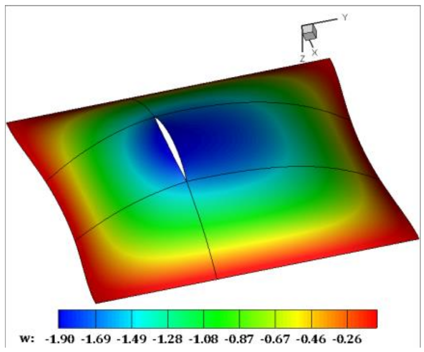

(c) 3D-deformation for plate with boundary conditions of type A at $P_xA^2/E_2h^3 = 9$

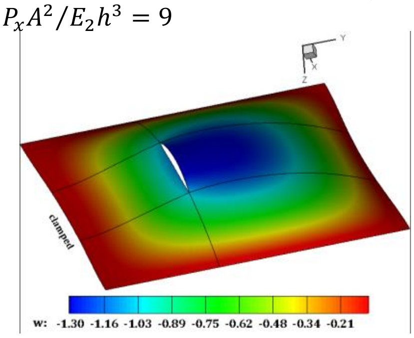

(d) 3D-deformation for plate with boundary conditions of type B at $P_xA^2/E_2h^3 = 9$

Fig. 31 Comparison between the results of laminates with both boundary conditions of types A and B (arrangement B)

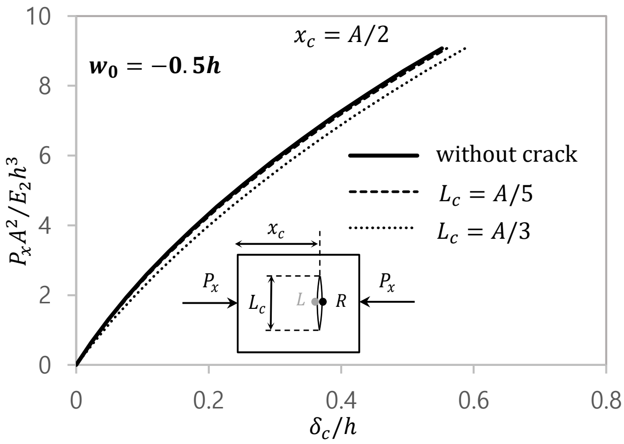

Fig. 32 Variations of load versus end shortening displacement for imperfect plates with initial imperfection of $-0.5h$ subjected to P_x with different lengths of crack (type A, arrangement A, $x_c = A/2$)

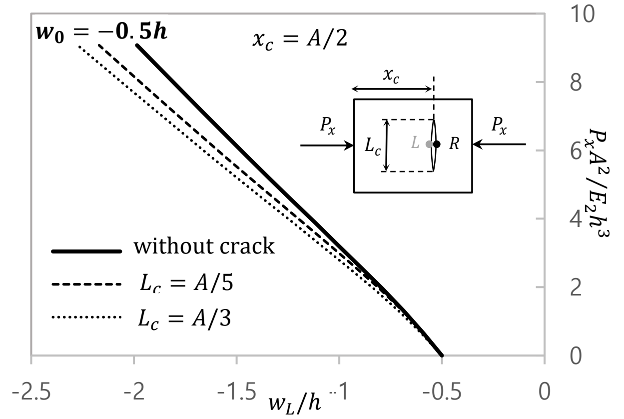

Fig. 33 Variations of load versus out-of-plane displacement for imperfect plates with initial imperfection of $-0.5h$ subjected to P_x with different lengths of crack (type A, arrangement A, $x_c = A/2$)

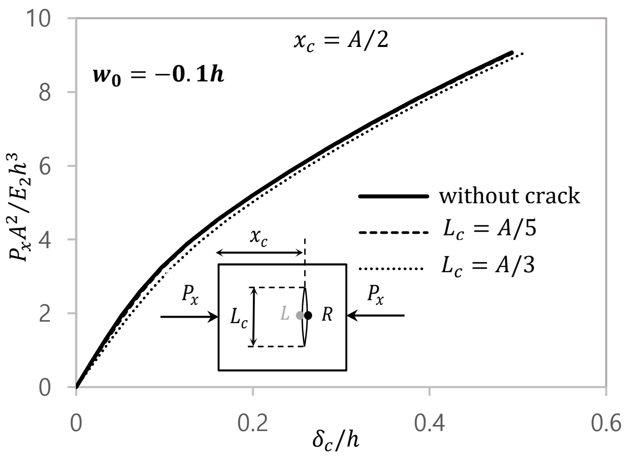

Fig. 34 Variations of load versus end shortening displacement for imperfect plates with initial imperfection of $-0.1h$ subjected to P_x with different lengths of crack (type A, arrangement A, $x_c = A/2$)

behaviors of imperfect laminates. Some selected results,

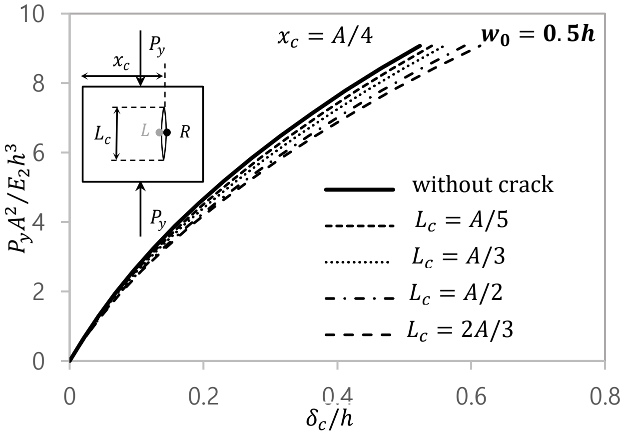

Fig. 38 Variations of load versus end shortening displacement for imperfect plates with initial imperfection of $0.5h$ subjected to P_y with different lengths of crack (type A, arrangement A, $x_c = A/4$)

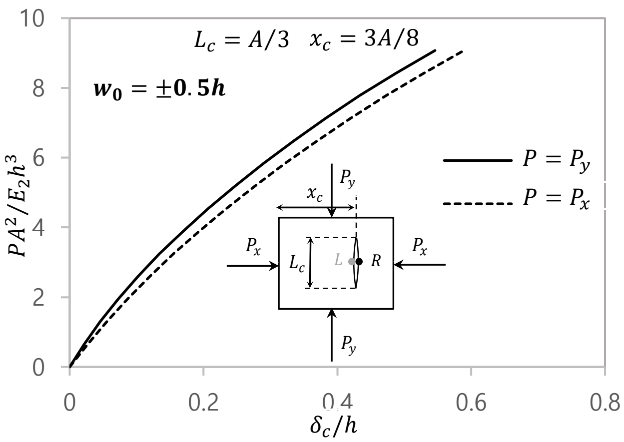

Fig. 39 Variations of load versus end shortening displacement for imperfect plates with initial imperfection of $\pm 0.5h$ subjected to compressive loads with different directions (type A, arrangement A, $x_c = 3A/8$, $L_c = A/3$)

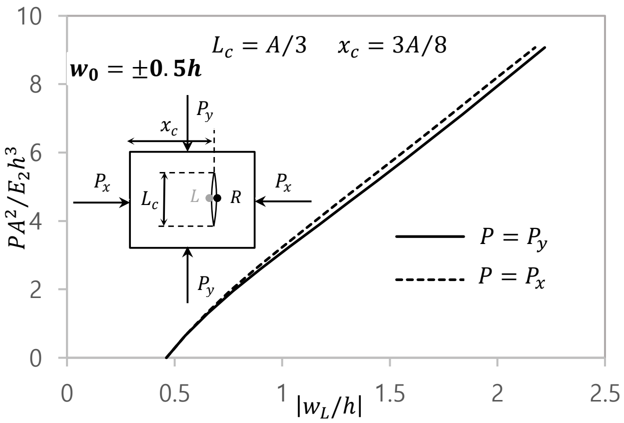

Fig. 40 Variations of load versus out-of-plane displacement for imperfect plates with initial imperfection of $\pm 0.5h$ subjected to compressive loads with different directions (type A, arrangement A, $x_c = 3A/8$, $L_c = A/3$)

including the variations of loads versus in-plane and out-of-

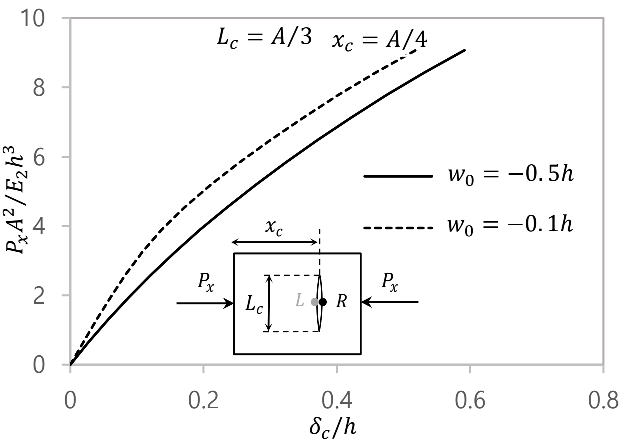

Fig. 41 Variations of load versus end shortening displacement for imperfect plates subjected to P_x with different initial imperfections (type A, arrangement A, $x_c = A/4,\ L_c = A/3$)

plane displacements with prescribed values of imperfection and for various lengths and locations of the crack, are depicted in Figs. 32-41. To do this, an initial sinusoidal imperfection has been assumed for both directions with amplitude of 10% and 50% of the plate thickness (i.e., $w_0 = 0.1h$ & $0.5h$).

The crack modeling is based on arrangement A and the boundary conditions of the laminates are assumed to be type A. As before, if the loading direction is along the *x*-direction, the crack axis is perpendicular to the loading, and if the compressive load is applied in the *y*-direction, the crack has been placed along the loading direction. The variations of loads versus end shortening and out-of-plane displacements for plates including the crack located at the center have been depicted in Figs. 32 to 37.

In Figs. 32 to 35, the results has been represented for different lengths of crack in the laminates subjected to in-plane compressive load P_x while the same study for plates subjected to compressive load P_y has been depicted in Figs. 36 and 37. Since the laminates under compressive load P_x start to deflect in negative direction, the amplitude of initial imperfection has been assumed to be $w_0 = -0.5h$ or $w_0 = -0.1h$ for these laminates while these values are assumed to be positive for laminates containing the crack along the loading direction.

In the results obtained for perfect plates, it was seen that when the crack axis is perpendicular to the loading direction, there is no significant effect on the nonlinear response of the laminate, while when it is along the loading direction, it completely affects the response of the plate. However, by observing the results of this section, it can be said that when the plates have an initial imperfection (especially with large amplitude), the effects of the crack are more evident, and these effects will also increase when the cracks are along the loading.

The stiffness degradation of an imperfect laminate with increasing the length of the crack can be seen in Fig. 38 when the crack is located at $x_c = A/4$ and the amplitude of initial imperfection is $0.5h$.

In order to observe the behavioral difference of the laminates containing crack and imperfection, under loading in both directions P_x or P_y, the nonlinear responses of these plates have been represented in Figs. 39 and 40. These plates have initial imperfections of $\pm 0.5h$ and the crack in these plates has been located at $x_c = 3A/8$ and the length of the crack is assumed to be $A/3$. The nonlinear response of an internally cracked imperfect laminate with two different values of initial imperfection can be observed in Fig. 41. As it can be seen, the nonlinear behavior of this laminate changes greatly by changing the value of initial imperfection.

5. Conclusions

The purpose of this research was to investigate the geometric nonlinear behavior of edge and internally cracked composite plates with or without initial imperfection. The Ritz method was used by Legendre polynomials for the primary variable approximations. To model the crack, a plate decomposition technique was applied and the penalty technique was used to enforce interface continuity between the sub-plates. In this research, different types of boundary conditions were assumed and the laminated plates were subjected to biaxial compressive loads and then a sensitivity analysis was done with respect to the applied load direction along the parallel and orthogonal to the crack axis. The results were presented for influence of crack length, various locations of crack, load direction, boundary conditions and initial imperfection values. It was observed that when the crack axis is perpendicular to the loading direction, there is no significant effect on the nonlinear response of the laminate, while when it is along the loading direction, it completely affects the response of the plate. Also, it was seen that when the plates have an initial imperfection, the effects of the crack are more evident even if the crack axis is perpendicular to the loading direction.

References

Alinia, M.M., Hosseinzadeh, S.A.A. and Habashi, H.R. (2007), "Influence of central cracks on buckling and post-buckling behaviour of shear panels", *Thin-Wall. Struct.*, **45**, 422-431.

Batra, R.C. and Ching, H.K. (2002), "Analysis of Elastodynamic deformations near a crack/notch tip by meshless local Petrov-Galarkin (MLPG) method", *Comput. Model. Eng. Sci.*, **3**(6), 717-730.

Cao, Z. and Liu, Y. (2012), "A new numerical modeling for evaluating the stress intensity factors in 3-D fracture analysis", *Struct. Eng. Mech.*, **43**(3), 321-336.

Cetkovic, M. and Vuksanovic, D. (2011), "Large deflection analysis of laminated composite plates using layerwise displacement model", *Struct. Eng. Mech.*, **40**(2), 257-277.

Chia, C.Y. (1988), "Geometrically nonlinear behavior of composite plates: A review", *Appl. Mech. Rev.*, **41**(12), 439-451.

Dimitri, R., Fantuzzi, N., Yong, L. and Tornabene, F. (2017), "Numerical computation of the crack development and SIF in composite materials with XFEM and SFEM", *Compos. Struct.*, **160**, 468-490.

Fantuzzi, N., Tornabene, F. and Viola, E. (2016), "Four-parameter functionally graded cracked plates of arbitrary shape: A GDQFEM solution for free vibrations", *Mech. Adv. Mater. Struct.*, **23**(1), 89-107.

Ghannadpour, S.A.M., Kurkaani Barvaj, A. and Tornabene, F. (2018), "A semi-analytical investigation on geometric nonlinear and progressive damage behavior of relatively thick laminated plates under lateral pressure and end-shortening", *Compos. Struct.*, **194**, 598-610.

Ghannadpour, S.A.M., Ovesy, H.R. and Zia-Dehkordi, E. (2015), "Buckling and post-buckling behaviour of moderately thick plates using an exact finite strip", *Comput. Struct.*, **147**, 172-180.

Kandasamy, R., Dimitri, R. and Tornabene, F. (2016), "Numerical study on the free vibration and thermal buckling behavior of moderately thick functionally graded structures in thermal environments", *Compos. Struct.*, **157**, 207-221.

Kar, V.R. and Panda, S.K. (2016), "Post-buckling behaviour of shear deformable functionally graded curved shell panel under edge compression", *Int. J. Mech. Sci.*, **115**, 318-324.

Kar, V.R. and Panda, S.K. (2017), "Postbuckling analysis of shear deformable FG shallow spherical shell panel under nonuniform thermal environment", *J. Therm. Stress.*, **40**(1), 25-39.

Kar, V.R., Mahapatra, T.R. and Panda, S.K. (2017), "Effect of different temperature load on thermal postbuckling behavior of functionally graded shallow curved shell panels", *Compos. Struct.*, **160**, 1236-1247.

Kar, V.R., Panda, S.K. and Mahapatra, T.R. (2016), "Thermal buckling behavior of shear deformable functionally graded single/doubly curved shell panel with TD and TID properties", *Adv. Mater. Res.*, **5**(4), 205-221.

Katariya, P.V and Panda, S.K. (2016), "Thermal buckling and vibration analysis of laminated composite curved shell panel", *Aircr. Eng. Aerosp. Technol.*, **88**(1), 97-107.

Katariya, P.V., Das, A. and Panda, S.K. (2018), "Buckling analysis of SMA bonded sandwich structure-using FEM", *IOP Confer. Ser.: Mater. Sci. Eng.*, **338**(1), 012035.

Katariya, P.V., Panda, S.K. and Mohapatra, T.R. (2017b), "Nonlinear thermal buckling behaviour of laminated composite panel structure including the stretching effect and higher-order finite element", *Adv. Mater. Res.*, **6**(4), 349-361.

Katariya, P.V., Panda, S.K., Hirwani, C.K., Mehar, K. and Thakara, O. (2017a), "Enhancement of thermal buckling strength of laminated sandwich composite panel structure embedded with shape memory alloy fibre", *Smart Struct. Syst.*, **20**(5), 595-607.

Kress, R. and Lee, K.M. (2003), "Integral equation methods for scattering from an impedance crack", *Comput. Appl. Math.*, **161**, 161-177.

Leissa, A.W. (1987), "A review of laminated composite plate buckling", *Appl. Mech. Rev.*, **40**, 575-591.

Liu, Y. and Shu, D.W. (2015), "Effects of edge crack on vibration characteristics of delaminated beam", *Struct. Eng. Mech.*, **53**(4), 767-780.

Milazzo, A. and Oliveri, V. (2015), "Post-buckling analysis of cracked multilayered composite plates by pb-2Rayleigh–Ritz method", *Compos. Struct.*, **132**, 75-86.

Milazzo, A. and Oliveri, V. (2017), "Buckling and post-buckling of stiffened composite panels with cracks and delaminations by ritz approach", *AIAA J.*, **55**, 965-980.

Monfared, M.M. (2017), "Mode III SIFs for interface cracks in an FGM coating-substrate system", *Struct. Eng. Mech.*, **64**(1), 71-79.

Nasirmanesh, A. and Mohammadi, S. (2015), "XFEM buckling analysis of cracked composite plates", *Compos. Struct.*, **131**, 333-343.

Ovesy, H.R. and Ghannadpour, S.A.M. (2009), "An exact finite strip for calculation of relative post-buckling stiffness of isotropic plates", *Struct. Eng. Mech.*, **31**(2), 181-210.

Ovesy, H.R. and Ghannadpour, S.A.M. (2011), "An exact finite strip for the initial postbuckling analysis of channel section struts", *Comput. Struct.*, **89**(19), 1785-1796.

Ovesy, H.R., Zia-Dehkordi, E. and Ghannadpour, S.A.M. (2016), "High accuracy post-buckling analysis of moderately thick composite plates using an exact finite strip", *Comput. Struct.*, **174**, 104-112.

Panda, S.K. and Ramachanda, L. (2011), "Buckling and post-buckling behavior of cross-ply composite plate subjected to non-uniform in-plane loads", *J. Eng. Mech.*, **137**(9), 589-597.

Panda, S.K., and Katariya, P.V. (2015), "Stability and free vibration behavior of laminated composite panels under thermo-mechanical loading", *Int. J. Appl. Comput. Math.*, **1**(3), 475-490.

Panda, S.K. and Singh, B.N. (2009), "Thermal postbuckling behavior of laminated composite cylindrical/hyperboloid shallow shell panel using nonlinear finite element method", *Compos. Struct.*, **91**(3), 366-374.

Panda, S.K. and Singh, B.N. (2010a), "Nonlinear free vibration analysis of thermally post-buckled composite spherical shell panel", *Int. J. Mech. Mater. Des.*, **6**(2), 175-188.

Panda, S.K. and Singh, B.N. (2010b), "Thermal post-buckling analysis of a laminated composite spherical shell panel embedded with shape memory alloy fibres using non-linear finite element method", *J. Mech. Eng. Sci.*, **224**(4), 757-769.

Panda, S.K. and Singh, B.N. (2011), "Large amplitude free vibration analysis of thermally post-buckled composite doubly curved panel using nonlinear FEM", *Fin. Elem. Analy. Des.*, **47**(4), 378-386.

Panda, S.K. and Singh, B.N. (2013a), "Nonlinear finite element analysis of thermal post-buckling vibration of laminated composite shell panel embedded with SMA fibre", *Aerosp. Sci. Technol.*, **29**(1), 47-57.

Panda, S.K. and Singh, B.N. (2013b), "Large amplitude free vibration analysis of thermally post-buckled composite doubly curved panel embedded with SMA fibers", *Nonlin. Dyn.*, **74**(1-2), 395-418.

Panda, S.K. and Singh, B.N. (2013c), "Post-buckling analysis of laminated composite doubly curved panel embedded with SMA fiber subjected to thermal environment", *Mech. Adv. Mater. Struct.*, **20**(10), 842-853.

Panda, S.K., Mohapatra, T.R. and Kar, V.R. (2017), *Nonlinear Finite Element Solution of Post-buckling Responses of FGM Panel Structure under Elevated Thermal Load and TD and TID Properties*, MATEC Web of Conferences 109, 05005.

Peng, L.X., Tao, Y., Liang, N., Li, L. and Teng, X. (2017), "Simulation of a crack in stiffened plates via a meshless formulation and FSDT", *Int. J. Mech. Sci.*, **131-132**, 880-890.

Rangarajan, R. and Gao, H. (2015), "A finite element method to compute three-dimensional equilibrium configurations of fluid membranes: Optimal parameterization", *J. Comput. Phys.*, **297**, 266-294.

Seifi, R. and Kabiri, A.R. (2013), "Lateral Load effects on buckling of cracked plates under tensile loading", *Thin-Wall. Struct.*, **72**, 37-47.

Seifi, R. and Khodayari, N. (2011), "Experimental and numerical studies on buckling of cracked thin-plates under full and partial compression edge loading", *Thin-Wall. Struct.*, **49**, 1504-1516.

Shahverdi, H. and Navardi, M.M. (2017), "Free vibration analysis of cracked thin plates using generalized differential quadrature element method", *Struct. Eng. Mech.*, **62**(3), 345-355.

Viola, E., Tornabene, F. and Fantuzzi, F. (2013a), "Generalized differential quadrature finite element method for cracked composite structures of arbitrary shape", *Compos. Struct.*, **106**, 815-834.

Viola, E., Tornabene, F., Ferretti, E. and Fantuzzi, F. (2013b), "GDQFEM numerical simulations of continuous media with cracks and discontinuities", *Comput. Model. Eng. Sci.*, **94**(4), 331-369.

Yang, Q.J., Hayman, B. and Osnes, H. (2013), "Simplified buckling and ultimate strength analysis of composite plates in compression", *Compos. Part B: Eng.*, **54**, 343-352.

Yuan, J. and Dickinson, S.M. (1992), "Flexural vibration of rectangular plate systems approached by using artificial springs in the Rayleigh-Ritz method", *J. Sound Vibr.*, **159**(1), 39-55.

CC